The feasibility of predicting the spatial pattern of soil particle-size distribution using a pedogenesis model

Yuxin Ma[a,*], Budiman Minasny[a], W.D. Dimuth P. Welivitiya[b,c], Brendan P. Malone[a], Garry R. Willgoose[b], Alex B. McBratney[a]

[a] Sydney Institute of Agriculture, School of Life and Environmental Sciences, The University of Sydney, NSW 2006, Australia
[b] School of Engineering, The University of Newcastle, NSW 2006, Australia
[c] School of Environment and Life Sciences, The University of Newcastle, NSW 2006, Australia

ARTICLE INFO

ABSTRACT

Particle-size distribution (PSD) plays an important role in influencing a number of soil physical, chemical, and biological properties. Currently, digital soil mapping (DSM) methods based on empirical observations have been widely used in mapping PSD. However, DSM methods rarely consider soil genetic processes. This paper investigated the use of a mechanistic soil evolution model, State Space Soil Production and Assessment Model (SSSPAM), to simulate the spatiotemporal evolution of PSD in the Hunter Valley, NSW, Australia. SSSPAM simulates the spatial and temporal variation of PSD within a landscape based on erosion due to overland flow, deposition, and physical weathering within the soil profile. We conducted a simulation over the 144 km^2 area using a 30 m digital elevation model (DEM) as an input. The model simulated soil evolution over 70,000 years to ensure that the PSD had reached steady-state. To validate and analyze the influence of different process parameters on particle size dynamics, we carried out a parametric study in a field within the study area and found a strong relationship between runoff excess generation, exponential weathering rate, and soil particle-size distribution. As expected, higher discharge rates produced coarser particles and larger weathering rates produced finer PSD. We further explored the feasibility of combining the mechanistic SSSPAM and empirical DSM approaches by comparing simulation results with observed sand content. We found limitations of the SSSPAM model to predict sand fraction accurately in the study area due to incomplete process coverage. The output of SSSPAM can be improved by integrating it with DSM techniques. Overall, SSSPAM can explore how particle size will change through time and identify areas with risks of erosion and deposition. Such a model can be used to inform large-scale management to ensure our soil is secured in the future.

1. Introduction

Particle-size distribution (PSD) is a fundamental and important soil attribute because it plays a key role in influencing a number of soil physical, chemical, and biological properties such as bulk density, hydraulic conductivity, water holding capacity, erodibility, carbon storage and many others (Van Looy et al., 2017; Minasny and McBratney, 2018). Soil texture, expressed by the relative proportions of sand, silt, and clay, is the most common descriptor of PSD and varies in space and time as soil evolves in response to weathering processes and sediment transport (Cohen et al., 2010). Understanding the spatial distribution and dynamic variability of soil texture is imperative in the quest for improved agricultural development that secures our soil (Zhao et al., 2009; Adhikari et al., 2013; Akpa et al., 2014).

In the past decade, the soil science community has formulated various statistical models in the digital soil mapping (DSM) framework to predict the spatial distribution of soil properties (e.g., Grimm et al., 2008; Viscara Rossel and Behrens, 2010). This statistical approach is based on empirical soil observations which are correlated to environmental covariates via various techniques, such as Regression Kriging, Generalised Linear Models (GLM) (Poggio et al., 2013), Generalised Addictive Models (GAM) (Scull et al., 2003), Cubist (Henderson et al., 2005; Ma et al., 2017), Random Forests (Hengl et al., 2015), artificial neural networks (Malone et al., 2009), Genetic Algorithm (Nelson and Odeh, 2009), support vector machine (Ahmad et al., 2010; Ballabio, 2009), Bayesian inference model and expert knowledge (Zhu et al., 1996, 2001). These methods fulfill the increasing need for quantitative soil information but are of limited use in complex terrain where
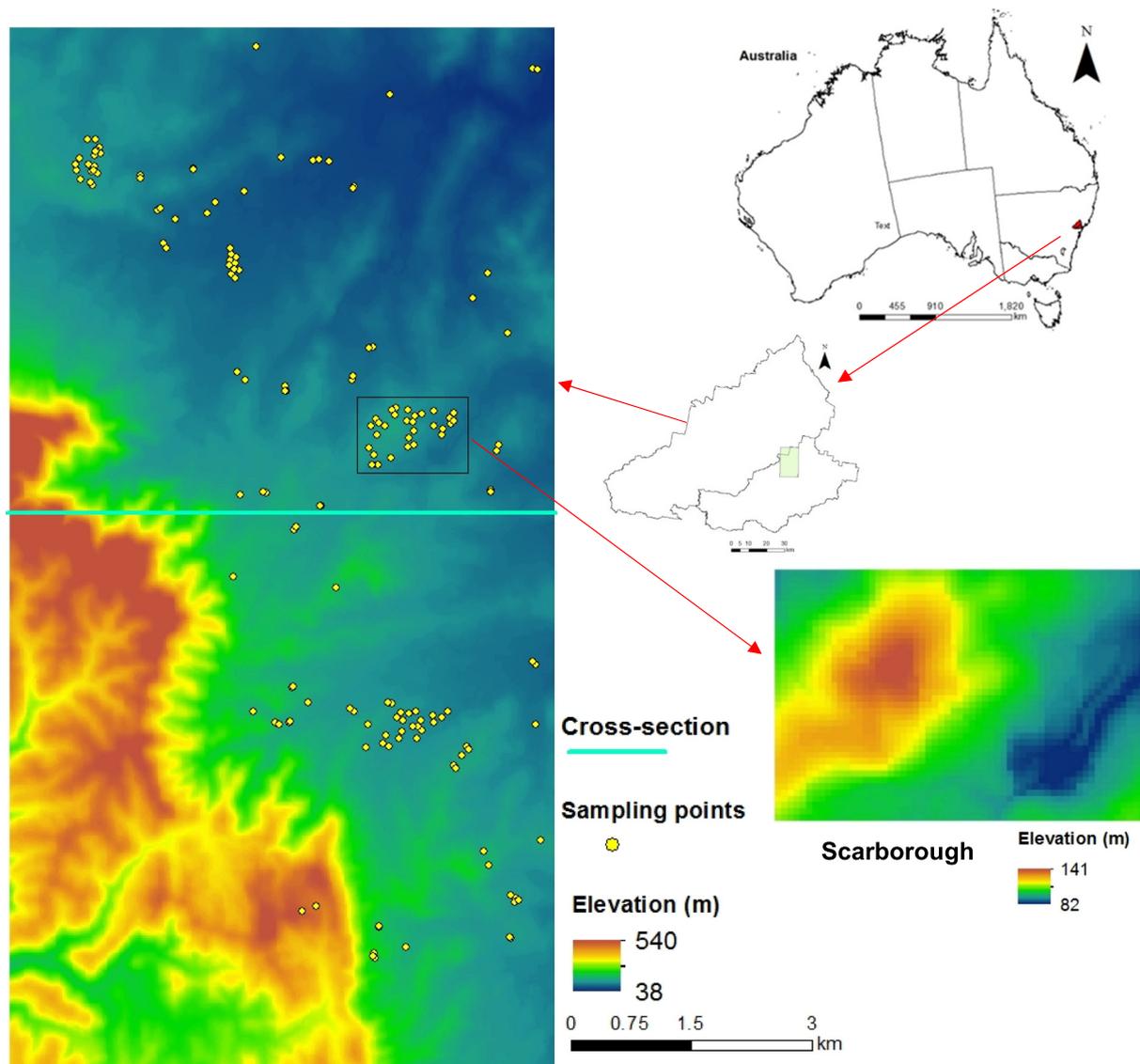
Fig. 1. Location of the study area in the Hunter Valley, Scarborough, and their DEM. The blue line represents a cross-section of the area for visualisation of the simulation. (For interpretation of the references to colour in this figure legend, the reader is referred to the web version of this article.)

observations are difficult to obtain. Moreover, DSM models assume that soil properties are in equilibrium with the landscape where they developed and rarely consider soil genetic processes. Simulating soil properties across the landscape ideally should be achieved by mechanistic models rather than using empirical models.

Researchers have found strong links between the soils and the landform on which they reside (Welivitiya et al., 2016). The dynamics of changes in soil attributes can have a significant impact on the long-term processes (landform evolution) and the spatial variability and magnitude of soil properties (Minasny et al., 2015). Conversely, landscape evolution influences soil development, i.e., erosion or deposition changes soil thickness (Bonfatti et al., 2018). Understanding the spatiotemporal variability of soil properties in a dynamic landform can best be achieved by a process-based soil-landscape evolution model. For example, MILESD (Model for Integrated Landscape Evolution and Soil Development) (Vanwalleghem et al., 2013) and LORICA (Temme and Vanwalleghem, 2016) incorporate various chemical and biological processes in the simulation. MILESD is built on the rudimentary framework of landscape-scale models for soil redistribution (Minasny and McBratney, 1999, 2001) and a pedon-scale soil formation model (Salvador-Blanes et al., 2007). LORICA modifies the three-layer module

to represent the soil profile in MILEDS to incorporate additional layers and combines with the landform evolution model LAPSUS (Schoorl et al., 2014). SSSPAM (State Space Soil Production and Assessment Model) extends these approaches to test more general conditions (Welivitiya, 2016).

This paper aims to explore the use of mechanistic pedogenesis model SSSPAM for modelling the spatiotemporal evolution of PSD across an area in the Hunter Valley, New South Wales, Australia. With the intention to improve the use of pedological knowledge in DSM techniques, we also tested the value of process-based model outputs as covariates in DSM to predict the spatial pattern of sand content.

2. Materials and methods

Willgoose and Sharmeen (2006) developed a physically-based model named ARMOUR to simulate spatial and temporal changes of armouring and weathering processes on a one-dimensional hillslope. However, this approach is infeasible for large-scale 2D or 3D soil evolution simulations due to the extensive computer resources and very long runtimes. By simplifying ARMOUR, Cohen et al. (2009) reformulated it as a state-space matrix model named mARM which is

capable of using the interaction between three layers to simulate soil particle-size evolution. Extending the mARM model, Cohen et al. (2010) then developed mARM3D which is able to model soil profile PSD employing a number of dynamic soil layers at a large spatial extent. However, such a model has not been used in extensive catchment scale simulations and detailed soil profile evolution. SSSPAM generalised and extended mARM3D, and coupled it with a landform evolution model.

SSSPAM simulated soil evolution over 70,000 years to reach equilibrium using a 30 m digital elevation model (DEM) as an input. The model considers erosion, deposition, and physical weathering over a 144 km^2 area. A parametric study was carried out in the Scarborough field which is located within the study area to explore the influences of erosion and physical weathering processes parameters in SSSPAM. We only conducted the parametric study in this field because of the relatively long computational time of the model (Keijsers et al., 2011; Schoorl et al., 2014). The sand content simulations using SSSPAM were compared with the results using DSM approach and observed texture data.

2.1. Study site

The study site is located in the Lower Hunter Valley, New South Wales, Australia. It is delimited by longitudes 151°13′26.04″ E – 151° 19′8.4″ E and latitudes 32°42′25.2″ S – 32°51′26.352″ S with a total area of about 144 km^2. This site is in the temperate climatic zone with warm, humid summers and cooler humid winters. The mean annual precipitation is over 750 mm. The underlying geology includes predominantly Early Permian siltstones, marl, and some minor sandstone (Hawley et al., 1995) and Late Permian siltstones, Middle Permian conglomerates, sandstones and siltstones in minor amounts (Malone et al., 2016a). Topographically the area is constituted mostly of undulating hills which ascend to low mountains in the southwest. Elevation ranges from 38 m to 540 m (Fig. 1). Land use is mainly dedicated to viticultural industry, followed by dryland agricultural grazing systems. The soils generally are weathered kaolinitic–smectitic type soils, ranging from light to medium texture grade. The dominant soil types are Dermosols, Calcarosols, and Chromosols (Australian Classification System, Isbell, 2002) or Chromic Luvisols, Dystric Nitosols, Dystric Regosols and Calcic Luvisols (according to WRB, FAO, 1998). Clay illuviation is therefore an important pedogenic process in the region.

2.2. Soil samples and soil analysis

The soil dataset we used contains 613 samples collected from different depths during different surveys (Odgers et al., 2011; Malone et al., 2014; Fajardo et al., 2015). In addition to the whole-area survey, detailed field-scale survey was also conducted in a field called Scarborough (area 1.72 × 10^6 m^2) (Fig. 1). Sample locations were recorded using a hand-held global position system (GPS) device (Garmin Map 76, Garmin Corporation). Samples were collected and brought back to the laboratory, air-dried at room temperature (20–22 °C). Stones/gravels and debris were removed and then sieved to pass a 2 mm sieve. The prepared soil samples were then stored in polyethylene bottles for analysis.

A portable visible-near infrared (vis-NIR) spectrophotometer, Agrispec with a Contact Probe attachment (Analytical Spectral Devices, Boulder Colorado), was used to scan the samples from 500 to 2500 nm with a Spectralon® white tile as a reference reflectance. Clay, defined as particles < 2 μm, silt (2–20 μm), and sand (20–2000 μm) according to International textural classifications, were predicted from the spectra based on a spectral library of soils from different locations in New South Wales, Australia (Chang et al., 2001; Cozzolino and Moron, 2003; Shepherd and Walsh, 2002). The coefficient of determination (R^2) and the concordance correlation coefficient (ρ_c) (Lin, 1989) were used to evaluate the performance of soil texture prediction model. The

validation for the prediction of sand content provided an R^2 value of 0.45 and ρ_c of 0.56. As the soil samples were collected from different depth ranges, mass preserving depth splines were fitted individually to each profile for the standardized depth intervals of 0–5, 5–15, 15–30, 30–60, and 60–100 cm. The vis-NIR predictions and spline fitted data were used as observations to fit in the DSM model.

2.3. SSSPAM model

SSSPAM is a state-space matrix model that simulate spatial and temporal variation of soil texture through a soil profile based on erosion due to overland flow, deposition, and physical weathering (exponential and humped models) within the profile which extends the approach of mARM and mARM3D (Welivitiya, 2016).

SSSPAM uses a matrix equation to represent physical processes and interactions between a number of layers. These layers are: 1) a water layer which transports material laterally, 2) a surface soil layer with direct contact with the overland flow, 3) several soil layers representing the soil profile and 4) a semi-infinite bedrock layer without weathering.

2.3.1. Model description

In SSSPAM, the state vector g defines the soil particle-size at any specific time in any layer. Entries g_i in the state vector g indicate the proportion of the material in the particle range i. In this study, there are 11 particle ranges. The alteration from one state to another state during a time step representing a process is defined using a transition matrix equation:

$$\boldsymbol{g}_{t_2} = R\boldsymbol{g}_{t_1} \tag{1}$$

where $\boldsymbol{g}_{t1}$ and $\boldsymbol{g}_{t2}$ are state vectors defining the soil texture at time t$_1$ and t$_2$. R is the marginal transition matrix.

2.3.2. Erosion and deposition process

In SSSPAM, the surface particle sizes change over time because of the selective movement of finer particles by erosion, resupply of the material from the subsurface and disintegration of particles due to physical weathering. The entrainment of particles at any time step from the surface is determined by the erosion transition matrix which is formulated by the Shield's shear stress threshold. The Shield's shear stress threshold determines the maximum particle size which can be transported in the overland water flow (Eq. (2)). A selective movement mechanism is used. In Willgoose and Sharmeen (2006), the mechanism was a good fit to field data when the particles are smaller than the Shield's shear stress threshold:

$$d_{th} = \frac{1}{F_s} \frac{\tau_0}{\gamma(s-1)} \tag{2}$$

where d_{th} (mm) is the maximum particle size that the flow (water) can dislodge from the surface layer, s is the specific gravity of the entrained particles (here we assume $s = 2.65$, dimensionless), γ is the unit weight of water (N/m^3) and F_s is the Shield's entrainment threshold (Henderson, 1966). The default value for F_s, used in this study, for non-cohesive and cohesive sediments is $F_s = 0.045$ (dimensionless), which is in the range recommended by a reanalysis of a large number of incipient motion studies for gravel-bed rivers (Buffington and Montgomery, 1997). τ_0 is the bed shear stress (N/m^2) which is given by

$$\tau_0 = \gamma R_h S \tag{3}$$

where R_h is the hydraulic radius (m) and S is the slope of the hillslope. R_h is the ratio of cross-section area and wetted perimeter. If R_h is large, a small area of water in the cross-section is affected by each meter of bed, so the friction effect of the bed is limited, and the efficiency is high, and vice versa.

The erosion rate E (m/s) of the surface is calculated from the flow shear stress and by a detachment-limited incision model. In the detachment-limited model, where the material is detached from the

surface and eroded by definition, there is no limit to the amount of sediment in transport. The erosion rate E (m/s) is:

$$E = e\frac{q^{\alpha_1}S^{\alpha_2}}{d_{50a}^{\beta}},$$ (4)

where e is the erodibility rate (dimensionless), q is the discharge rate per unit width (m^3/s/m), S is Slope, d_{50a} is the median diameter of the material in the surface layer (mm), α_1, α_2 and β are calibration exponents governing erosion process. α_1, α_2 can be derived from the shear stress-dependent erosion physics (Willgoose et al., 1991) or calibrated to field data. In this paper, we set α_1, α_2, β, e to 1.0, 1.2, 1.0 and 0.025, same as those of Cohen et al. (2009). For a one-dimensional hillslope with a unit width, the discharge at a particular point is simply calculated by

$$q = c_q rx,$$ (5)

where x is the distance down the slope from the uppermost point of the slope (m) and r is the runoff excess generation (m^3/s) (here $r = 4.7 \times 10^{-8}\,\text{m}^3/\text{s}$) (Cohen et al., 2009). In this study, c_q is a parameter for modifying the discharge rate. Materials eroded will be deposited down the slope based on the direction of water flow. More detailed description of the erosional and depositional processes can be found in Welivitiya (2016).

2.3.3. Physical weathering process

In SSSPAM, the weathering module includes two aspects: (1) the weathering mechanism for the disintegration of soil particles, and (2) the weathering rate of each soil layer which typically depends on the depth below the soil surface.

The breakdown of the particles in the surface and underlying subsurface layers is also modelled by a weathering transition matrix which defines the change in soil texture due to the fracturing of particles through physical weathering. Weathering is mass-preserving when larger particles split into smaller particles. Wells et al. (2008) found that a simple symmetric fracture model with two equal volume daughter particles best fitted their laboratory weathering experiments. The assumption is that a parent particle with diameter d breaks into a single daughter particle with diameter d_1 and $n - 1$ smaller daughter particles with diameter d_2.

$$d^3 = d_1^3 + (n-1)d_2^3;$$ (6)

If the single larger particle with diameter d_1 accounts for α fraction of the parent particle, then

$$d_1 = \alpha^{\frac{1}{3}}d;$$ (7)

$$d_2 = \left(\frac{1-\alpha}{n-1}\right)^{\frac{1}{3}}d$$ (8)

It is possible to simulate various fragmentation geometries by changing the α fraction value and the number of daughter particles n. For instance, a symmetric fracture mechanism with two daughter particles ($\alpha = 0.5$, $n = 2$) and an asymmetric fracture mechanism ($\alpha = 0.99$, $n = 11$) where a large daughter has 99% of the parent particle volume, and ten smaller daughters retain 1% of the parent particle volume.

Before examining the effect of depth dependency of weathering, we need to distinguish two separate, but potentially related, weathering processes: 1) soil production (bedrock weathering) rate (Heimsath et al., 1997), at which bedrock is converted to soil materials, occurring at the bedrock-interface; 2) soil weathering rate (Wells et al., 2006; Yoo and Mudd, 2008), at which large soil particles break down into smaller particles.

The assumption is that weathering rate decreases as the soil depth increases, which is based on the well-established inverse relationship between soil production rate and soil thickness (Torrent and Nettleton, 1978; Muhs, 1984; Stockmann et al., 2014). Two commonly discussed

soil production functions are translated here into weathering functions of both bedrock and soil: (1) exponential depth-dependent weathering functions (Ahnert, 1977; Heimsath et al., 1997), and (2) humped exponential depth-dependent weathering functions (Ahnert, 1977; Minasny and McBratney, 2006). In the exponential model, the weathering rate is largest at the surface and decreases as a function of depth exponentially. The rationale is that physical weathering rates are most greatly affected by wetting, drying, and temperature cycles (Wells et al., 2005, 2006; Stockmann et al., 2014) which are typically strongest closer to the surface and decline with depth (Burke et al., 2007). The exponential function $f_{(h)}^{exp}$ used is:

$$f_{(h)}^{exp} = \beta' e^{(-\delta_1 h)};$$ (9)

where h (m) is the soil layer depth below the surface, β' is a constant defining the maximum weathering rate and δ_1 is the depth scaling factor. Here $\beta' = 1$, $\delta_1 = 1.738$.

The humped function has the largest weathering rate close to the surface at some nonzero depth and then decreases exponentially below that depth. The rationale of this function is that the weathering rate is highest when water accumulates on some thickness of soil. The humped exponential function $f_{(h)}^{hum}$ is:

$$f_{(h)}^{hum} = \frac{P_0\left[e^{(-\delta_2 h + \delta_4)} - e^{(-\delta_3 h)}\right]}{M};$$ (10)

where P_0 (m/yr) is the maximum weathering rate, h (m) is the thickness of the soil layer below the surface, δ_2, δ_3, and δ_4 are constants to characterize the shape of the function, M is the maximum value (i.e., the peak of the hump) to normalize the function. The values proposed by Minasny and McBratney (2006) of $P_0 = 0.25$, $\delta_2 = 4$, $\delta_3 = 6$ and $M = 0.04$ are used here. δ_4 is 0.02 to create a function that asymptotes close to 0 (Cohen et al., 2010).

In SSSPAM, it is also currently not possible to run the combination of both depth dependent weathering functions (exponential and humped). Thus, the profile can only be simulated assuming one process. In this paper, the weathering rate of each layer is determined by modifying the nominal weathering rate W_0 (1.5×10^{-3}/yr) and the exponential depth-dependent weathering function $f_{(h)}^{exp}$ with a parameter c_w. The weathering rate of a soil layer at a depth of h from surface W_h (has units of 1/time) is given by

$$W_h = c_w W_0 f_{(h)}^{exp}$$ (11)

2.3.4. Inputs to SSSPAM

The current DEM derived from SRTM data at a spatial resolution of 30 m was used as an initial value in the SSSPAM model. In SSSPAM, the catchment is discretized into a regular grid of pixels that each have an altitude value representing the surface topography. In this study, for each pixel, eleven soil layers were defined representing a surface layer (0–5 cm) and ten subsurface layers (5–105 cm) each with a thickness of 10 cm. Bedrock starts under the bottom soil layer. Both soil layers and bedrock are assumed initially homogeneous. The initial soil surface and subsurface particle size distribution datasets were created based on the study of Welivitiya et al. (2016). In each layer, 100% of the material was assumed to be the coarsest particle-size class (> 4 mm), which represents the initial situation dominated by gravel/rock. Using the above input data, the SSSPAM model simulated soil evolution over 70,000 years with particle-size output every 100 years. We ran the model over this period to ensure that the particle-size distribution had reached a steady-state condition, typically before 100,000 years (Welivitiya et al., 2016).

2.4. Digital soil maps

Digital soil maps of soil texture were produced using spatial prediction functions of soil particle size distribution based on observed soil

texture coupled with environmental covariates using the Cubist regression model. The digital maps were compared to SSSPAM model outputs.

Cubist is a rule-based model which has been found to be quite effective in digital soil mapping (Malone et al., 2016b). It is a tree model algorithm based on the M5 theory (Quinlan, 1992) and partitions the predictor variates into different subsets according to "if-then" rules (Kuhn et al., 2016). In this study, we fitted 100 Cubist models using random samples with replacement in the R statistical software to extract mean prediction of sand and clay content.

A number of environmental covariates were considered in this study including Landsat 7 with the Enhanced Thematic Mapper Plus (ETM+) and terrain attributes derived from the DEM, i.e. slope, aspect, terrain ruggedness index (TRI), terrain position index (TPI), topographic wetness index (TWI), Multiresolution Index of Valley Bottom Flatness (MrVBF), Multiresolution Ridge Top Flatness (MrRTF), Slope Length and Steepness Factor (LS-factor), Relative Slope Position (RSP), valley depth. All covariates were used at a spatial resolution of 30 m.

2.5. Model comparison

To explore the feasibility of using SSSPAM output for mapping particle size, we compared its performance with observed texture data. In this study, we explore four possible models:

(a) Predictions of DSM using the Cubist model. Observed soil texture was coupled with a number of environmental covariates. We extracted the mean prediction values of sand content and compared the contributions of the environmental predictors.
(b) The simulated surface d50 value for 0–5 cm and simulated profile d50 value for 35–55 and 55–105 cm respectively were added as an additional covariate in digital soil mapping. Then we used the same method as in (a) to predict the sand content and compared the model performance between (a) and (b).
(c) Predictions using the SSSPAM model.
(d) Residuals were calculated as the difference between observed sand content and the predicted value from SSSPAM. Residuals were then modelled using DSM technique using the same method as in (a). This exercise is to identify covariates that can be used to enhance the performance of SSSPAM. Finally, the modelled residuals were added to the SSSPAM simulations (c) to explore the performance of the combination of DSM and SSSPAM model.

3. Results

3.1. Parametric study of SSSPAM

The nominal parameters used are presented in Table 1 based on the study of Welivitiya et al. (2016). The values of one parameter at a time were varied while keeping all others stable and the model was repeatedly run for sensitivity analysis of parameters.

Table 1
Parameters used in the simulation.

	Parameter	Value	Equation no
Erosion parameters	α_1	1.0	4
	α_2	1.2	4
	β	1.0	4
	e	0.025	4
	r	$4.7 \times 10^{-8}\,\mathrm{m^3/s}$	5
	c_q	1.0, 10.0	5
Weathering parameters	α	0.5	6
	n	2.0	6
	W_0	1.5×10^{-3}/yr	11
	c_w	0.1, 10.0	11

Erosion is a function of local discharge, slope, and the median diameter (d50) of the soil surface as indicated in Eq. (4) and is assumed to be detachment-limited which means that material is eroded by definition and there is no transport limitation (Temme and Vanwalleghem, 2016). To simulate a more humid climate, the runoff generation parameter in Eq. (5) was set to be 1 and 10. Fig. 2(a) and (b) shows the steady state d50 value generated for a surface with a combination of different runoff rates and weathering.

It is obvious that a higher discharge rate produces coarser surface particles and reduced discharge rate produces a finer surface. In Scarborough, at a higher discharge rate, the Shield's stress threshold increases and larger particles (sand and gravel) can be eroded from the surface. Meanwhile, the weathering rate remains constant which is unable to breakdown the surface fast enough, leading to a coarser surface layer. At a lower discharge rate, the Shield's stress threshold decreases, thus allowing smaller particles to be retained in the surface layer. Moreover, the erosion rate decreases while the weathering rate remains unchanged which makes weathering become more dominant. Both of these processes produce a finer surface.

Fig. 2(c) and (d) shows that the equilibrium d50 value decreases with a combination of different weathering and erosion intensity. Higher weathering rates break down the larger particles more rapidly. As weathering produces fine particles at the surface layer, they can be eroded. Subsequently, the surface layer was replaced by new weathered materials leading to a finer surface (Fig. 2(d)). This result is consistent with the finding of Welivitiya et al. (2016). Under limited erosion rate, when the weathering rate is elevated to 10 times, the model produces a uniform fine soil material at the surface across the field (d50 values < 0.5 mm).

3.2. Median diameter (d50) distribution

To understand the profile development, the equilibrium surface (0–5 cm) and subsurface (5–105 cm) d50 distribution of the study area were simulated (Fig. 3) using the parameters listed in Table 1 (c_q and c_w = 1.0) and the exponential weathering functions. Clearly, the northeastern area is dominated by fine materials (d50 < 2.0 mm), while the south-western mountainous region is characterized by gravel in both surface and subsurface. The simulated PSD that d50 is small in the north-eastern and large in the south-western region is consistent with the current land use. The land in the north-eastern region has been dedicated for dryland agricultural grazing system and expansive viticultural industry. In contrast, tracts of remnant natural vegetation (dry forest) are apparent, particularly toward the south-western of the study area (Bell, 2004). On the hillslope, high erosion and weathering rates produce a coarser surface compared to the subsurface profile where the effect of water erosion is less prominent. On the plains, materials from the higher elevation area were deposited, causing a finer soil surface.

3.3. The evolution of d50

The SSSPAM model allows us to visualise how the particles evolved and elevation changed with time through weathering, erosion and deposition processes. Fig. 4(a) shows the initial condition for the soilscape which consists of the gravel/rock of the whole soil profile. The evolution of soil and landscape along a cross-section of the area is presented in Fig. 4(b)–(d).

Initially, the erosion-dominated and deposition-dominated regions can be clearly identified. In the erosion-dominated region, the erosion is largest at the top of the hillslope and reduces gradually down the slope, causing a reduction in the elevation. On the hillslope, the water flow is capable of entraining materials from the surface due to the large transport capacity. This erosion process causes a sharp increase of the surface d50 at the top of the hillslope. Erosion rate decreases down the slope due to saturation of the flow with upstream sediments. At the bottom of the hill, the weathering process produces fine particles faster
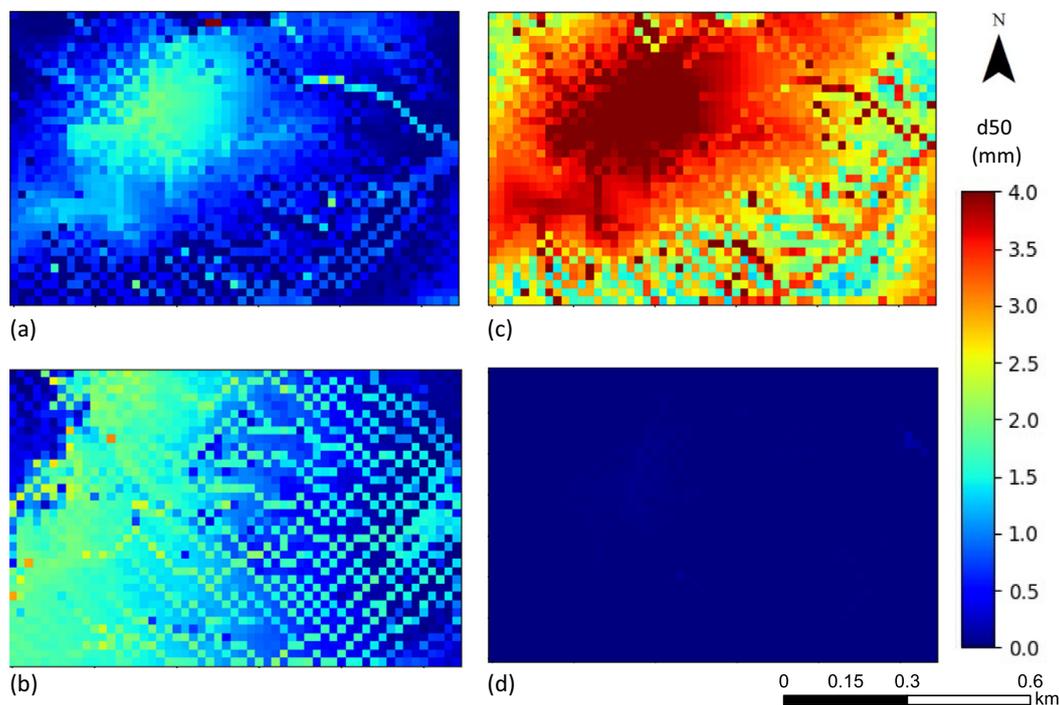
Fig. 2. The equilibrium d50 (mm) values for the surface layer (0–5 cm) simulated by SSSPAM for different runoff rates in Scarborough (a: $c_w = 1$, $c_q = 1$; b: $c_w = 1$, $c_q = 10$) and at different exponential weathering rates (c: $c_q = 1$, $c_w = 0.1$; d: $c_q = 1$, $c_w = 10$).

than the erosion rate which causes a decrease of the d50 at the surface with time. In the deposition-dominated region, fine particles were retained at the surface because of the low transport capacity of the water flow. Deposition caused an increase in elevation.

It becomes apparent that the limitation of this simulation is that we use the current DEM as input. Clearly, the erosion process has levelled much variation leading to the current undulating hills with the highest elevation about 540 m (Fig. 1) to a smooth hillslope (elevation < 400 m). On the other hand, in areas with elevation < 150 m, there is no significant change of elevation due to the erosion and weathering processes. It is clear that the spatial pattern of soil particle-size

distribution in these latter areas would be more realistic.

3.4. Identifying erosion risk areas

In the previous section, we have discussed the influence of different runoff rates. According to the downscaled 10 km rainfall projections from the NSW and ACT Regional Climate Modelling (NARCliM) project, the mean annual rainfall erosivity in NSW is predicted to increase in the future compared with the baseline period (1990–2009). Statewide, there is about a 7% increase in the near future (2020–2039) (Yang et al., 2015). Thus, some areas will have a higher erosion risk due to the
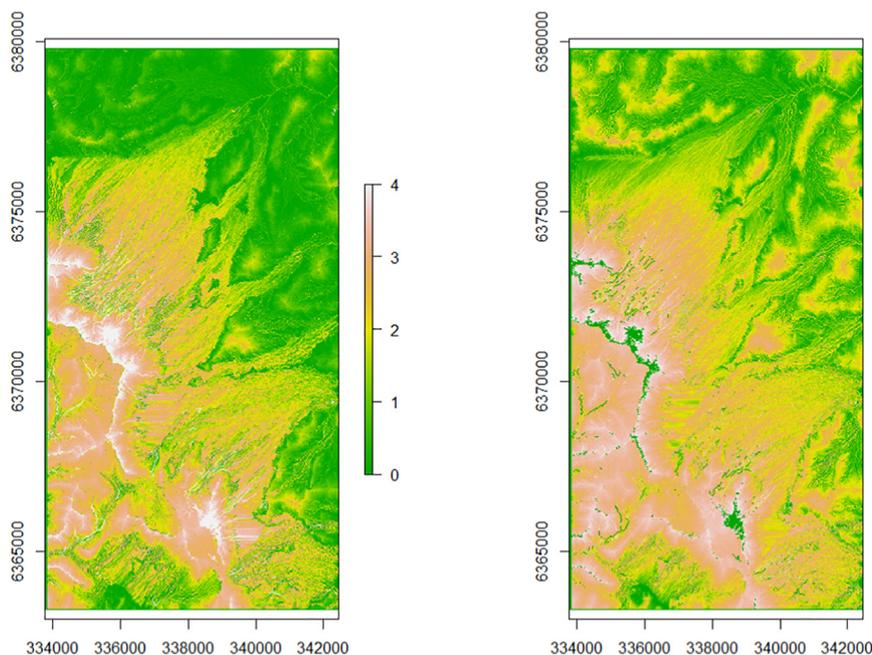

Fig. 3. The SSSPAM simulation of median diameter d50 (mm) in the surface (0–5 cm) (left) and subsurface (5–105 cm) (right).
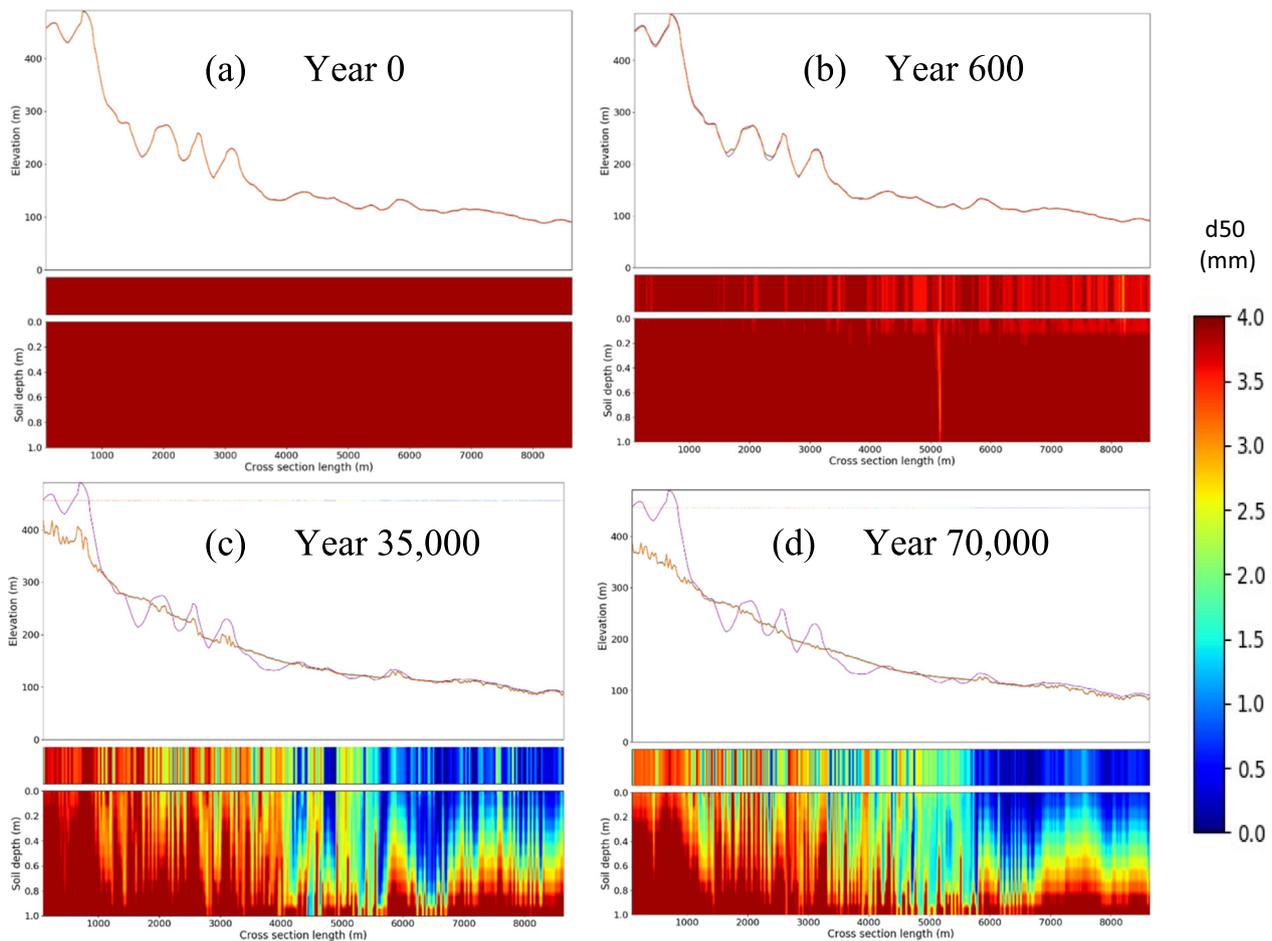
Fig. 4. A cross-section over the study area showing the evolution of median diameter (d50) of particles. In each of the panels, the upper section is the elevation of the soil profile and the landform, with the purple line denoting the original soil and landscape surface. The middle section is the median diameter d50 of the soil surface. The bottom section is the d50 distribution of subsurface profile relative to the surface. (For interpretation of the references to colour in this figure legend, the reader is referred to the web version of this article.)

increased rainfall intensity. Fig. 5 shows the predicted future change in d50 (mm) value for the near future (the next 20 years) when the original erosion rate is elevated to 10 times in SSSPAM. The change in d50 value on the hill summits region and areas with the lowest elevation in the study area remains around 0.05 mm. That is because intensive rainfall removes fine particles consistently from the original gravel-oriented hillslope top, which causes it to remain coarse. Fine particles are deposited in the valleys, making the surface remain to be fine.

According to the predicted change in PSD, we can recognize areas with increased erosion risk (identified as an increase of d50 between 0.05 and 2.85 mm) and deposition areas (area with d50 decrease between −2.82 and −0.05 mm). Under high rainfall intensity, finer particles are removed from the upslope, and deposited down the hillslope, causing the increase of d50 on the top and decrease of d50 at the bottom of the hillslope. In the flat parts, with elevation < 150 m, some areas like Scarborough we discussed before, are in danger under intensive rainfall scenario. Identifying these erosion risk areas has implications for water quality, crop productivity, vineyard management due to the significance of the regions and their current erosion levels. Simulation maps produced from SSSPAM over a decadal period would be useful for continuous soil condition monitoring and management.

3.5. Predicting sand content

Based on Smeck et al. (1981) and Chittleborough et al. (1984), no fine clay is formed through physical weathering, so here we will focus on the prediction of sand content. The simulated steady-state results of

the SSSPAM model show that the entire study area is characterized by a high level of sand content in the surface layer (0–5 cm) and moderate content in subsurface layers (35–55, 55–105 cm) (Fig. 6). In general, the sand content is found to increase from the south to north in all layers and decrease with increasing depth along the profile.

The northern, eastern, north-eastern and south-eastern zones in the study area are the areas with higher sand content in both surface and subsurface layers. On the contrary, the sand content in the southwest mountainous region is lower than the other parts of the surface layer because the hillslope areas are dominated by gravel (the white parts in Fig. 6).

The main reason for the higher sand content in the surface is that the largest physical weathering rate broke the larger particles more rapidly. As the weathering front moved farther from the surface, the pedogenic rate declined with increasing soil thickness due to the self-limiting nature of the pedogenic processes (Vanwalleghem et al., 2013). That is why the subsurface layers in the mountainous region were still dominant by gravel/rock in equilibrium (Fig. 6). Moreover, chemical weathering of soil particles was found to be the strongest at the weathering front close to the bedrock (Yoo and Mudd, 2008). The lack of chemical weathering processes in this model may cause the poor predictions of the subsurface layers.

3.6. Spatial modelling of sand content

To be able to spatially predict sand content for the whole area, we compared four different models: predictions using DSM with the Cubist
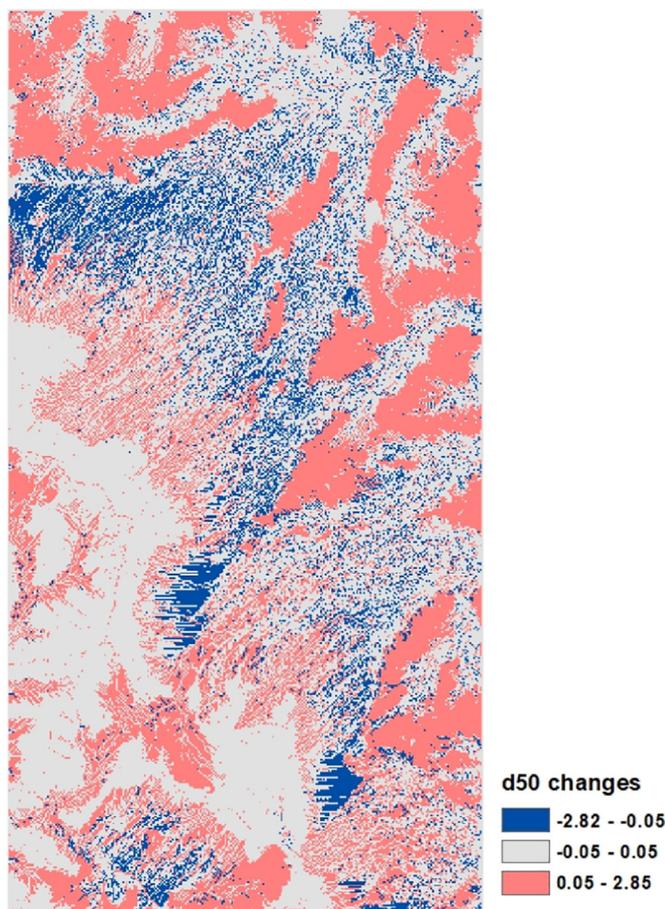
Fig. 5. The change in d50 (mm) value for surface (0–5 cm) after 20 years under ten times runoff rates in SSSPAM.

model (Fig. 7(a)), predictions using DSM with simulated d50 value as an additional covariate (Fig. 7(b)), predictions using SSSPAM model (Fig. 7(c)), and SSSPAM simulations with modelled residuals (Fig. 7(d)). The statistics of the observations are shown in Table 2 and the locations of samples are given in Fig. 7.

3.6.1. DSM products

In the north-eastern part, sand contents vary largely for surface and slightly for the sub-surface (Fig. 7(a)). In the south-western

mountainous region, sand content was predicted to be between 40% and 50%. However, there is a large uncertainty in the mountainous region because of a lack of observations. For DSM prediction, the sand content is large (mean value of 44%) for 0–5 cm and small for 35–55 (mean of 34%), 55–105 cm (mean of 37%) with R^2 values: 0.45, 0.33, and 0.36, respectively (Table 3). This is because soils observed at most sampling points were characterized by texture contrast soils. The high clay subsoil is due to clay translocation (eluviation–illuviation) processes which removed clays from surface layers and deposited them in the subsoil (coarse-over-fine profile). The Cubist regression model indicates that valley depth, LS-factor, and Relative Slope Position (RSP) were the largest contributing factors in the prediction, indicating that texture is governed mostly by transport process-related factors without the consideration of other factors like land use.

3.6.2. Comparison of SSSPAM with observed data and DSM products

SSSPAM simulations (Fig. 7(c)) produce a surface with relatively large sand content (mean value of 49%), however, the median particle size increases with depth (high gravel content) (see details in Fig. 6). This is because SSSPAM only considers physical processes with the assumption of bedrock uniformity, without considering chemical weathering and translocation of clay. In addition, transport process is limited by a detachment-limited incision model. Compared to observations that were mainly texture contrast soils, SSSPAM simulations have quite low R^2 values (0.13, 0.01, and 0.04 for 0–5, 35–55, 55–105 cm) (Table 3), indicating that SSSPAM cannot predict the sand content accurately. Nevertheless, SSSPAM provides predictions in the hillslope area (high gravel contents), which DSM cannot achieve without soil samples.

3.6.3. Using SSSPAM as a covariate

We used the d50 value from SSSPAM simulation as an additional covariate in DSM (Fig. 7(b)). The sand content predicted from this combined model has a mean value of 40% for 0–5 cm, 32% for 35–55 cm and 38% for 55–105 cm with R^2 values of 0.48, 0.32, and 0.37. The R^2 values only increase slightly for surface and remain almost constant for subsurface compared with original DSM (Table 3). In reference to the distribution patterns, it is obvious that there is almost no difference for subsurface and slight differences for surface with the additional covariate (d50). In this way, we might not be able to prove the usefulness of process-based model prediction in DSM.

3.6.4. Identifying soil formation processes not covered by SSSPAM

Calculating residual as the difference between observed sand content and the predicted value from SSSPAM and combining modelled
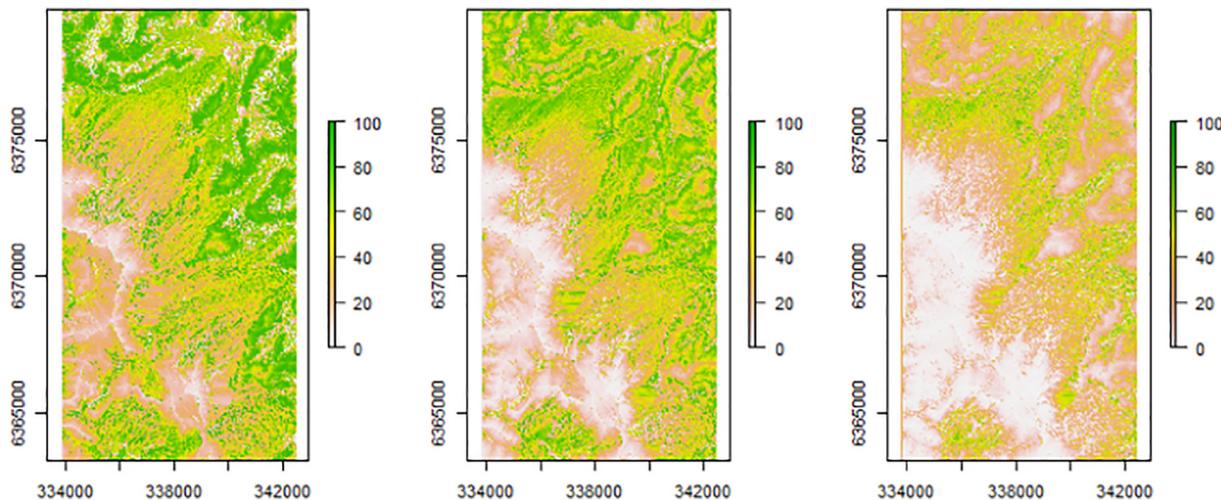

Fig. 6. The SSSPAM simulation of sand content (%) in 0–5 cm, 35–55 cm, 55–100 cm under steady-state condition.
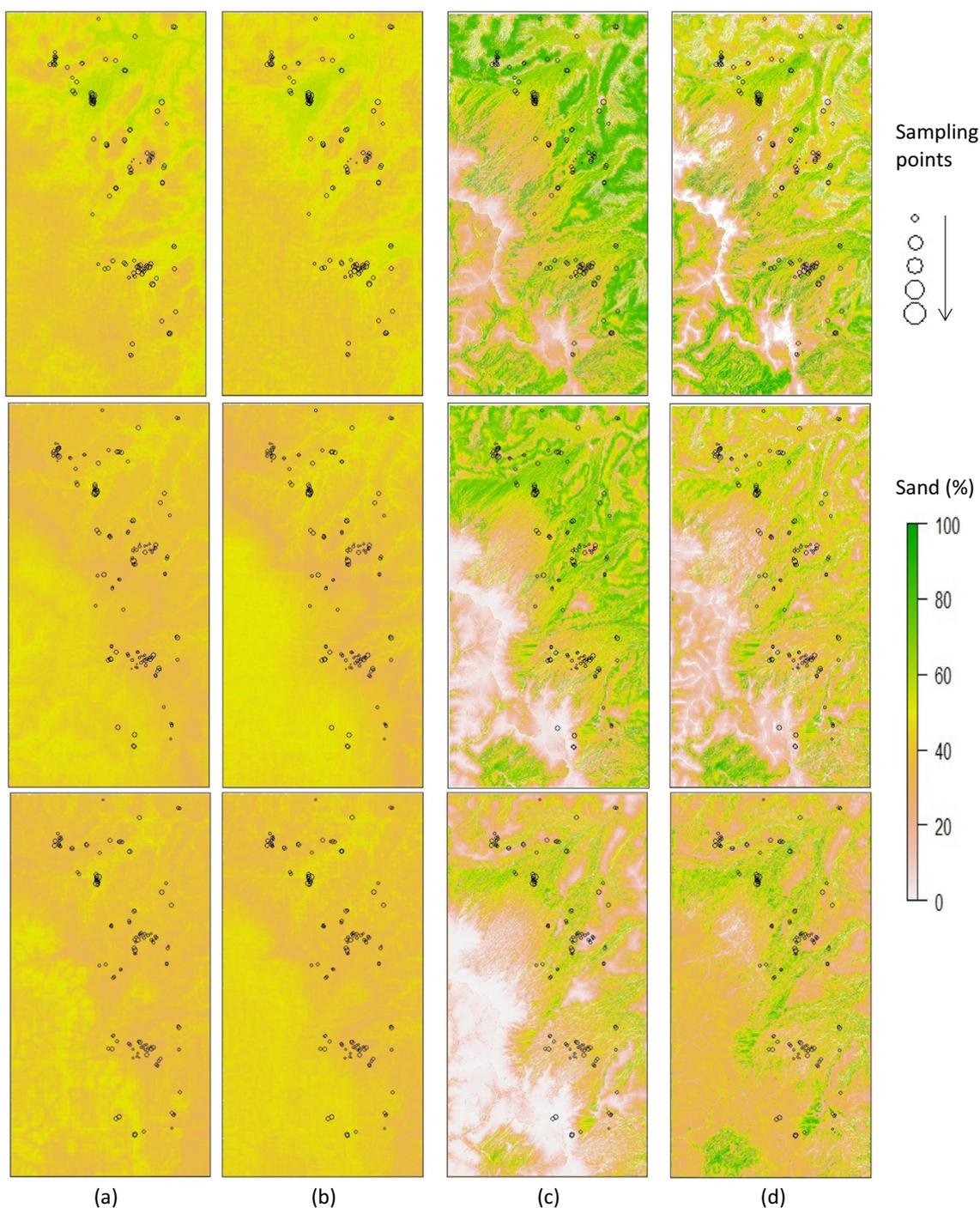
Fig. 7. Predictions of sand content (%) using (a) DSM, (b) DSM + d50 as an additional covariate, (c) SSSPAM, (d) SSSPAM + DSM of residual (Top to Bottom: 0–5 cm, 35–55 cm, 55–105 cm). The different values of observations are represented by the size of circles.

Table 2
The mean and standard deviation of sand and clay observations (%).

Depth	Sand	Clay
0–5 cm	46.3 ± 7.2	25.0 ± 6.6
35–55 cm	38.9 ± 8.9	39.0 ± 6.9
55–105 cm	39.3 ± 8.3	37.6 ± 7.0

Table 3
The R^2 values of different models.

Depth	DSM	SSSPAM	DSM + d50 as additional covariate	SSSPAM + DSM of residual
0–5 cm	0.45	0.13	0.48	0.52
35–55 cm	0.33	0.01	0.32	0.32
55–105 cm	0.36	0.04	0.37	0.38

residual using DEM and SSSPAM simulations, we can see that R^2 values (0.52, 0.32, and 0.38 for 0–5, 35–55, 55–105 cm) increase significantly for both surface and subsurface compared to the original SSSPAM

simulations (Table 3). In the mountainous areas, both Fig. 7(c) and (d) show the gravel pattern of the surface, whereas Fig. 7(d) reveals the clay dominated subsoil.

Comparing all the figures, R^2 values of Fig. 7(d) are the highest, and the spatial patterns are the most detailed. Thus, we may conclude that SSSPAM can be improved by DSM techniques because of the high performance of process-related covariates in the Cubist model, such as valley depth (100%), LS-factor (100%) and RSP (100%). On the other hand, we can solve the limitation of DSM in areas with difficulties in sampling (mountainous region) using SSSPAM to get an appropriate prediction.

3.7. Assumptions and limitations

In this paper, we have only considered a uniform bedrock parent material using the current DEM and modelling physical weathering mechanisms with a constant weathering rate. We only discussed sand simulation in this paper due to the difficulty in the formulation of fine clay through physical weathering. Moreover, we did not measure gravel content for the observed samples, and there were no samples in the high elevation areas. That will be one reason for reduced accuracy and precision of DSM and SSSPAM results and their comparison. Thus, there is a need to explicitly model variable weathering rates for different particle size classes at each time step (Vanwalleghem et al., 2013; Salvador-Blanes et al., 2007) and incorporate chemical and biological weathering (Green et al., 2006; Lin, 2011; Riebe et al., 2004; Roering et al., 2002; Vanwalleghem et al., 2013). Another important aspect needed is accounting for the effect of land use, not just the erosion from the overland water flow.

4. Conclusions

In this study, we predicted the spatial pattern and evolution of particle size using the mechanistic pedogenesis model SSSPAM and compared its sand content prediction with a DSM model. It can be concluded that:

1) SSSPAM simulations are profiles with a high sand content on the surface and high gravel contents in subsoils. SSSPAM can explore how the particle size will change through time and identify areas with risks of erosion and deposition.

2) The SSSPAM model should be further developed to simulate the equilibrium soil distribution. In this paper, we just took into account physical processes. There is a need to incorporate chemical weathering, bioturbation, clay translocation, neoformation of clay with time explicitly.

3) The SSSPAM model can be improved by DSM techniques. We should build a 4-dimensional (three spatial and one temporal dimension) soil-landscape model based on pedological knowledge of soil processes and combine the empirical spatial data with the pedological knowledge to predict soils in space and time in subsequent studies.

References

Adhikari, K., Kheir, R.B., Greve, M.B., Bøcher, P.K., Malone, B.P., Minasny, B., McBratney, A.B., Greve, M.H., 2013. High-resolution 3-D mapping of soil texture in Denmark. Soil Sci. Soc. Am. J. 77, 860–876.

Ahmad, S., Kalra, A., Stephen, H., 2010. Estimating soil moisture using remote sensing data: a machine learning approach. Adv. Water Resour. 33, 69–80.

Ahnert, F., 1977. Some comments on the quantitative formulation of geomorphological processes in a theoretical model. Earth Surf. Process. Landf. 2, 191–201.

Akpa, S.I.C., Odeh, I.O.A., Bishop, T.F.A., Hartemink, A.E., 2014. Digital mapping of soil particle-size fractions for Nigeria. Soil Sci. Soc. Am. J. 78, 1953–1966.

Ballabio, C., 2009. Spatial prediction of soil properties in temperate mountain regions using support vector regression. Geoderma 151 (3–4), 338–350.

Bell, S.A.J., 2004. Vegetation of Werakata National Park, Hunter Valley, New South Wales. Cunninghamia 8 (3), 331–347.

Bonfatti, B.R., Hartemink, A.E., Vanwalleghem, T., Giasson, E., 2018. A mechanistic model to predict soil thickness in a valley area of Rio Grande do Sul, Brazil. Geoderma 309, 17–31.

Buffington, J.M., Montgomery, D.C., 1997. A systematic analysis of eight decades of incipient motion studies, with special reference to gravel-bedded rivers. Water Resour. Res. 33, 1993–2030.

Burke, B., Heimsath, A.M., White, A.F., 2007. Coupling chemical weathering with soil production across soil mantled landscapes. Earth Surf. Process. Landf. 32, 853–873.

Chang, C.W., Laird, D.A., Mausbach, M.J., Hurburgh Jr., C.R., 2001. Near-infrared reflectance spectroscopy-principal components regression analyses of soil properties. Soil Sci. Soc. Am. J. 65 (2), 480–490.

Chittleborough, D.J., Walker, P.H., Oades, J.M., 1984. Textural differentiation in chronosequences from eastern Australia: I. Description, chemical properties and micromorphology of soils. Geoderma 32, 181–202.

Cohen, S., Willgoose, G.R., Hancock, G.R., 2009. The mARM spatially distributed soil evolution model: a computationally efficient modeling framework and analysis of hillslope soil surface organization. J. Geophys. Res. Earth Surf. 114, F03001.

Cohen, S., Willgoose, G.R., Hancock, G.R., 2010. The mARM3D spatially distributed soil evolution model: three-dimensional model framework and analysis of hillslope and landform responses. J. Geophys. Res. Earth Surf. 115, F04013.

Cozzolino, D., Moron, A., 2003. The potential of near-infrared reflectance spectroscopy to analyse soil chemical and physical characteristics. J. Agric. Sci. 140, 65–71.

Fajardo, M., McBratney, A.B., Whelan, B., 2015. Fuzzy clustering of Vis–NIR spectra for the objective recognition of soil morphological horizons in soil profiles. Geoderma 263, 244–253.

FAO, 1998. World Reference Base for Soil Resources. Rome.

Green, E.G., Dietrich, W.E., Banfield, J.F., 2006. Quantification of chemical weathering rates across an actively eroding hillslope. Earth Planet. Sci. Lett. 242, 155–169.

Grimm, R., Behrens, T., Märker, M., Elsenbeer, H., 2008. Soil organic carbon concentrations and stocks on Barro Colorado Island-digital soil mapping using random forests analysis. Geoderma 146, 102–113.

Hawley, S., Glen, R., Baker, C., 1995. Newcastle Coalfield Regional Geology 1: 100 000. Geological Survey of New South Wales, Sydney, Australia.

Heimsath, A.M., Dietrich, W.E., Nishiizumi, K., Finkel, R.C., 1997. The soil production function and landscape equilibrium. Nature 388, 358–361.

Henderson, F.M., 1966. Open Channel Flow. Macmillan, New York.

Henderson, B.L., Bui, E.N., Moran, C.J., Simon, D.A.P., 2005. Australia-wide predictions of soil properties using decision trees. Geoderma 124 (3–4), 383–398.

Hengl, T., Heuvelink, G.B.M., Kempen, B., Leenaars, J.G.B., Walsh, M.G., Shepherd, K.D., Sila, A., MacMillan, R.A., Jesus, J.M., Tamene, L., Tondoh, J.E., 2015. Mapping soil properties of Africa at 250 m resolution: random forests significantly improve current predictions. PLoS One 10 (6), e0125814.

Isbell, R.F., 2002. The Australian Soil Classification. CSIRO Publishing, Melbourne.

Keijsers, J., Schoorl, J., Chang, K.T., Chiang, S.H., Claessens, L., Veldkamp, A., 2011. Calibration and resolution effects on model performance for predicting shallow landslide locations in Taiwan. Geomorphology 133 (3), 168–177.

Kuhn, M.K., Weston, S., Keefer, C., Coulter, N., 2016. Cubist Models for Regression.

Lin, L.I.K., 1989. A concordance correlation coefficient to evaluate reproducibility. Biometrics 45 (1), 255–268.

Lin, H., 2011. Three principles of soil change and pedogenesis in time and space. Soil Sci. Soc. Am. J. 75, 2049–2070.

Ma, Y.X., Minasny, B., Wu, C.F., 2017. Mapping key soil properties to support agricultural production in Eastern China. Geoderma Reg. 10, 144–153.

Malone, B.P., McBratney, A.B., Minasny, B., Laslett, G.M., 2009. Mapping continuous depth functions of soil carbon storage and available water capacity. Geoderma 154, 138–152.

Malone, B.P., Minasny, B., Odgers, N.P., McBratney, A.B., 2014. Using model averaging to combine soil property rasters from legacy soil maps and from point data. Geoderma 232, 34–44.

Malone, B.P., Sanjeev, K.J., Minasny, B., McBratney, A.B., 2016a. Comparing regression-based digital soil mapping and multiple-point geostatistics for the spatial extrapolation of soil data. Geoderma 262, 243–253.

Malone, B.P., Minasny, B., McBratney, A.B., 2016b. Using R for Digital Soil Mapping. Springer, pp. 133–136.

Minasny, B., McBratney, A.B., 1999. A rudimentary mechanistic model for soil production and landscape development. Geoderma 90, 3–21.

Minasny, B., McBratney, A.B., 2001. A rudimentary mechanistic model for soil production and landscape development II. A two-dimensional model incorporating chemical weathering. Geoderma 103, 161–179.

Minasny, B., McBratney, A.B., 2006. Mechanistic soil-landscape modelling as an approach to developing pedogenetic classifications. Geoderma 133, 138–149.

Minasny, B., McBratney, A.B., 2018. Limited effect of organic matter on soil available water capacity. Eur. J. Soil Sci. 69, 39–47.

Minasny, B., Finke, P., Stockmann, U., McBratney, A.B., 2015. Resolving the integral connection between pedogenesis and landscape evolution. Earth Sci. Rev. 150, 102–120.

Muhs, D.R., 1984. Intrinsic thresholds in soil systems. Phys. Geogr. 5, 99–110.

Nelson, M.A., Odeh, I.O.A., 2009. Digital soil class mapping using legacy soil profile data: a comparison of a genetic algorithm and classification tree approach. Aust. J. Soil Res. 47, 632–649.

Odgers, N., McBratney, A.B., Minasny, B., 2011. Bottom-up digital soil mapping. I. Soil layer classes. Geoderma 163, 38–44.

Poggio, L., Gimona, A., Brewer, M.J., 2013. Regional scale mapping of soil properties and their uncertainty with a large number of satellite-derived covariates. Geoderma 209–210, 1–14.

Quinlan, J.R., 1992. Learning with continuous classes. In: Proc. of the Fifth Australian Joint Conference on Artificial Intelligence World Scientific, Singapore, pp. 343–348.

Riebe, C.S., Kirchner, J.W., Finkel, R.C., 2004. Erosional and climatic effects on long-term chemical weathering rates in granitic landscapes spanning diverse climate regimes. Earth Planet. Sci. Lett. 224, 547–562.

Roering, J.J., Almond, P., Tonkin, P., McKean, J., 2002. Soil transport driven by biological processes over millennial time scales. Geology 30, 1115–1118.

Salvador-Blanes, S., Minasny, B., McBratney, A.B., 2007. Modeling long-term in-situ soil profile evolution—application to the genesis of soil profiles containing stone layers. Eur. J. Soil Sci. 58, 1535–1548.

Schoorl, J.M., Temme, A.J.A.M., Veldkamp, T., 2014. Modelling centennial sediment waves in an eroding landscape – catchment complexity. Earth Surf. Process. Landf. 39, 1526–1537.

Scull, P., Franklin, J., Chadwick, O.A., McArthur, D., 2003. Predictive soil mapping: a review. Prog. Phys. Geogr. 27 (2), 171–197.

Shepherd, K.D., Walsh, M.G., 2002. Development of reflectance spectral libraries for characterization of soil properties. Soil Sci. Soc. Am. J. 66, 988–998.

Smeck, N.E., Ritchie, A., Wilding, L.P., Drees, L.R., 1981. Clay accumulation in sola of poorly drained soils of western Ohio. Soil Sci. Soc. Am. J. 45, 95–102.

Stockmann, U., Minasny, B., McBratney, A.B., 2014. How fast does soil grow? Geoderma 216, 48–61.

Temme, A.J.A.M., Vanwalleghem, T., 2016. LORICA – a new model for linking landscape and soil profile evolution: development and sensitivity analysis. Comput. Geosci. 90, 131–143.

Torrent, J., Nettleton, W.D., 1978. Feedback processes in soil genesis. Geoderma 20, 281–287.

Van Looy, K., Bouma, J., Herbst, M., Koestel, J., Minasny, B., Mishra, U., et al., 2017. Pedotransfer functions in Earth system science: challenges and perspectives. Rev. Geophys. 55, 1199–1256.

Vanwalleghem, T., Stockmann, U., Minasny, B., McBratney, A.B., 2013. A quantitative model for integrating landscape evolution and soil formation. J. Geophys. Res. Earth Surf. 118 (2), 331–347.

Viscara Rossel, R.A., Behrens, T., 2010. Using data mining to model and interpret soil diffuse reflectance spectra. Geoderma 158 (1–2), 46–54.

Welivitiya, W.D.D.P., 2016. A Next Generation Spatially Distributed Model for Soil Profile Dynamics and Pedogenesis (PhD Thesis). The University of Newcastle, Australia.

Welivitiya, W.D.D.P., Willgoose, G.R., Hancock, G.R., Cohen, S., 2016. Exploring the sensitivity on a soil area-slope-grading relationship to changes in process parameters using a pedogenesis model. Earth Surf. Dyn. 4, 607–625.

Wells, T., Binning, P., Willgoose, G.R., 2005. The role of moisture cycling in the weathering of a quartz chlorite schist in a tropical environment: findings of a laboratory simulation. Earth Surf. Process. Landf. 30, 413–428.

Wells, T., Binning, P., Willgoose, G.R., Hancock, G.R., 2006. Laboratory simulation of the salt weathering of schist: I. Weathering of schist blocks in a seasonally wet tropical environment. Earth Surf. Process. Landf. 31, 339–354.

Wells, T., Willgoose, G.R., Hancock, G.R., 2008. Modelling weathering pathways and processes of the fragmentation of salt weathered quartz-chlorite schist. J. Geophys. Res. Earth Surf. 113, F01014.

Willgoose, G.R., Sharmeen, S., 2006. A one-dimensional model for simulating armouring and erosion on hillslopes: 1. Model development and event-scale dynamics. Earth Surf. Process. Landf. 31, 970–991.

Willgoose, G.R., Bras, R.L., Rodriguez-Iturbe, I., 1991. A physical explanation of an observed link area-slope relationship. Water Resour. Res. 27, 1697–1702.

Yang, X., Yu, B., Zhu, Q.G., 2015. Climate change impacts on rainfall erosivity and hillslope erosion in NSW. In: 21st International Congress on Modelling and Simulation, Gold Coast, Australia.

Yoo, K., Mudd, S.M., 2008. Discrepancy between mineral residence time and soil age: implications for the interpretation of chemical weathering rates. Geology 36 (1), 35–38.

Zhao, Z.Y., Chow, T.L., Rees, H.W., Qi, Y., Xing, Z.S., Meng, F.R., 2009. Predict soil texture distributions using an artificial neural network model. Comput. Electron. Agric. 65 (1), 36–48.

Zhu, A.X., Band, L.E., Dutton, B., Nimlos, T.J., 1996. Automated soil inference under fuzzy logic. Ecol. Model. 90, 123–145.

Zhu, A.X., Hudson, B., Burt, J., Lubich, K., Simonson, D., 2001. Soil mapping using GIS, expert knowledge, and fuzzy logic. Soil Sci. Soc. Am. J. 65, 1463–1472.